

Room-temperature magnetoelectric coupling in single-phase BaTiO₃-BiFeO₃ system

Su-Chul Yang,¹ Ashok Kumar,¹ Valeri Petkov,² and Shashank Priya^{1,a)}

¹Center for Energy Harvesting Materials and Systems (CEHMS), Bio-inspired Materials and Devices Laboratory (BMDL), Virginia Tech, Blacksburg, Virginia 24061, USA

²Department of Physics, Central Michigan University, Mount Pleasant, Michigan 48859, USA

(Received 13 February 2013; accepted 18 March 2013; published online 8 April 2013)

In this paper, single-phase multiferroic ceramics of $(1-x)$ BaTiO₃ - x BiFeO₃ (BT - x BFO) were synthesized by solid-solution method in the wide range of material composition ($x = 0.025 - 1.0$). The changes in crystal structure were confirmed via X-ray diffractions (XRD) and atomic pair distribution functions (PDFs). The room-temperature ME coupling was found to exhibit significant magnitude in the narrow composition window ($x = 0.71 - 0.8$) where the average crystal structure was found to be rhombohedral. Especially, the BT - 0.725 BFO ceramics containing local monoclinic distortions within rhombohedral phase were found to exhibit high room-temperature ME coefficient (α_{ME}) of 0.87 mV/cm·Oe with high piezoelectric properties ($g_{33} = 18.5 \times 10 \text{ mV m N}^{-1}$ and $d_{33} = 124 \text{ pC N}^{-1}$). We believe that the high room-temperature ME coupling in single-phase lead-free BT-BFO ceramics provides a possibility of developing electrically or magnetically tunable thin-film devices. © 2013 American Institute of Physics. [<http://dx.doi.org/10.1063/1.4799591>]

I. INTRODUCTION

Magnetoelectric (ME) multiferroics with coexisting ferroelectric and ferromagnetic ordering have gained attention as they provide the opportunity for developing tunable devices.¹⁻⁵ In past decade, many studies have focused on single-phase multiferroic materials such as Cr₂O₃ ($T_n = 307 \text{ K}$, $0.74 \text{ mV cm}^{-1} \text{ Oe}^{-1}$), LiCoPO₄ ($5.52 \text{ mV cm}^{-1} \text{ Oe}^{-1}$), TbPO₄ ($T_n = 2.27 \text{ K}$, $6.62 \text{ mV cm}^{-1} \text{ Oe}^{-1}$), YIG ($5.41 \text{ mV cm}^{-1} \text{ Oe}^{-1}$), BiFeO₃ ($T_c = 1103 \text{ K}$, $T_n = 643 \text{ K}$), BiMnO₃ ($T_c = 450 \text{ K}$, $T_n = 100 \text{ K}$), YMnO₃ ($T_c = 640 \text{ K}$, $T_n = 100 \text{ K}$), and BaMnF₄ ($T_n = 26 \text{ K}$).⁶⁻¹² Among these single-phase multiferroics, BiFeO₃ has attracted most attention due to its simultaneous ferroelectric and antiferromagnetic characteristics exhibiting high Curie temperature and high Neel temperature.¹³⁻¹⁶ However, high electric leakage in bulk BiFeO₃ ceramics was observed due to the existence of multivalent Fe ions and oxygen vacancies. To improve ferroelectric properties, studies on solid solution of BiFeO₃ with other perovskite materials (BaTiO₃, PbTiO₃, CaTiO₃, and Bi_{0.5}Na_{0.5}TiO₃) have been performed.¹⁷⁻²³ BaTiO₃ is a promising candidate in this respect, and $(1-x)$ BaTiO₃ - x BiFeO₃ solid solutions have been shown to exhibit rhombohedral ($0.7 < x \leq 1.0$), pseudo-cubic ($0.04 < x \leq 0.7$), and tetragonal ($0 \leq x \leq 0.04$) phases.²⁴ Moreover, substitution of La, Nb, and Mn in the BaTiO₃-BiFeO₃ has been studied in order to enhance the piezoelectric properties and DC resistivity.²⁵⁻²⁸ Recently, improved piezoelectric value of $d_{33} = 116 \text{ pC N}^{-1}$ with high DC resistivity of $2.7 \times 10^7 \text{ } \Omega \text{ m}$ was reported in Mn-modified BaTiO₃-BiFeO₃ ceramics by Leontsev *et al.*²⁸ In parallel, several studies on BaTiO₃-BiFeO₃ ceramics have shown that the solid solutions with BaTiO₃ results in enhanced magnetic properties. At room temperature, high

magnetic properties ($H_c = 660 \text{ Oe}$, $M_r = 0.75 \text{ emu g}^{-1}$, and M_s at $50 \text{ kOe} = 1.88 \text{ emu g}^{-1}$) were reported in $0.2 \text{ BaTiO}_3 - 0.8 \text{ BiFeO}_3$ ceramics by Park *et al.*²⁹

Generally, ME effect can be classified as direct magnetoelectric (DME) effect and converse magnetoelectric (CME) effect. The DME effect (dE_{AC}/dH_{AC}) is defined as the change in electric polarization in response to applied magnetic field. The CME (dB_{AC}/dE_{AC}) effect is defined as the change in magnetization in response to applied electric field. For single-phase multiferroic materials, figure-of-merit for ME coupling is given as:

$$\alpha_{ij} < (\epsilon_{ii}\mu_{jj})^{1/2},$$

where ϵ and μ are the electric permittivity and magnetic permeability, respectively. Thus, to achieve strong ME coupling in single-phase multiferroics, we need to find an optimum composition with high piezoelectric and magnetic properties.

In this study, we synthesized lead-free $(1-x)$ BaTiO₃ - x BiFeO₃ ceramics (BT - x BFO) by solid-solution method over the wide range of composition ($x = 0.025 - 1.0$) to find the optimum point for high ME coupling at room-temperature. Piezoelectric, magnetic, and magnetoelectric properties were investigated for all the compositions at room temperature.

II. EXPERIMENTAL DETAILS

Without any additional doping, all BT- x BFO ceramics were synthesized by mixed oxide sintering method using analytical reagent grade $\sim 99.9\%$ pure oxide and carbonate powders of TiO₂, Bi₂O₃, Fe₂O₃, and BaCO₃ from Ward Hill, USA. The sintered BT- x BFO ceramics had diameter of 10 mm and thickness of 1 mm. Crystal structures were investigated at room temperature using X-ray diffractometer (D/MAX-2500, Rigaku). The ceramics were poled in silicone oil for 30 min at room temperature under applied DC

^{a)}Author to whom correspondence should be addressed. Electronic mail: spriya@vt.edu.

electric field of 3.5 kV mm^{-1} and aged afterwards for 24 h at room temperature. Room-temperature ME responses were investigated under an applied magnetic bias field ($H_{\text{DC}} = 2000 \text{ Oe}$ with $H_{\text{AC}} = 1 \text{ Oe}$ at 1 kHz). Piezoelectric characteristics were examined using APC YE 2730 A d_{33} meter. Dielectric characteristics were investigated using HP 4194 A impedance analyzer (Hewlett Packard Co. USA). Ferroelectric polarization-electric field (P - E) measurement was performed using modified Sawyer-Tower Bridge Precision II (Radiant Technologies, Albuquerque, NM). Magnetization-magnetic field (M - H) measurement was performed using the vibrating sample magnetometer (VSM 7304, Lake Shore Cryotronics).

III. RESULTS AND DISCUSSION

Fig. 1(a) shows the room-temperature X-ray diffraction (XRD) patterns for BT- x BFO ($x = 0.025 - 1.0$) ceramics. The XRD patterns illustrate that the BT- x BFO exhibits tetragonal ($x = 0.025$), cubic ($x = 0.1 - 0.7$) and rhombohedral ($x = 0.8 - 1.0$) phases across the whole range of composition. We next focussed on the crystal structures of compositions corresponding to BT- x BFO ($x = 0.710 - 0.775$) shown in Fig. 1(b), where optimum ME coupling was found (shown later). The XRD pattern for pure BFO ($x = 1.0$) exhibited rhombohedral phase with splitting in the peaks of (110),

(111), (210), and (211). On modification with BT, the splitting gradually disappeared as BFO mole fraction decreased from $x = 1.0$ to $x = 0.725$. With further decrease in BFO mole fraction to $x = 0.71$, the peaks showed negligible splitting. The peaks shifted to lower 2θ values with BT modification in BFO ceramics due to the substitution of large ionic radii Ba^{2+} (1.35 \AA) ion on A-site and Ti^{4+} (0.68 \AA) ion on B-site as compared to the Bi^{3+} (1.08 \AA) and Fe^{3+} (0.64 \AA) ion, respectively. Figs 1(c) and 1(d) show the lattice parameter (a), rhombohedral distortion angle (α), and volume of unit cell for the BT- x BFO ($x = 0.71 - 0.775$ and 1.0). It was found that with decreasing BFO mole fraction the lattice parameter a increased from 3.956 \AA ($x = 1.0$) to 3.986 \AA ($x = 0.71$) and the distortion angle α increased and peaked at 89.99° ($x = 0.725$). The volume of unit cell increased from 61.90 \AA^3 ($x = 1.0$) to 63.31 \AA^3 ($x = 0.725$) with decreasing BFO mole fraction.

Figs. 2(a)–2(h) show the composition dependence of magnetoelectric, piezoelectric, and dielectric properties of BT- x BFO ceramics at room temperature. From Figs. 2(a) and 2(b), it can be noted that the DME effect was enhanced with proportional change of α_{DME} phase angle in the limited range of BT- x BFO compositions ($x = 0.71 - 0.8$) and the maximum α_{DME} ($0.87 \text{ mV cm}^{-1} \text{ Oe}^{-1}$) was observed at the optimum composition of BT- x BFO ($x = 0.725$). As shown in

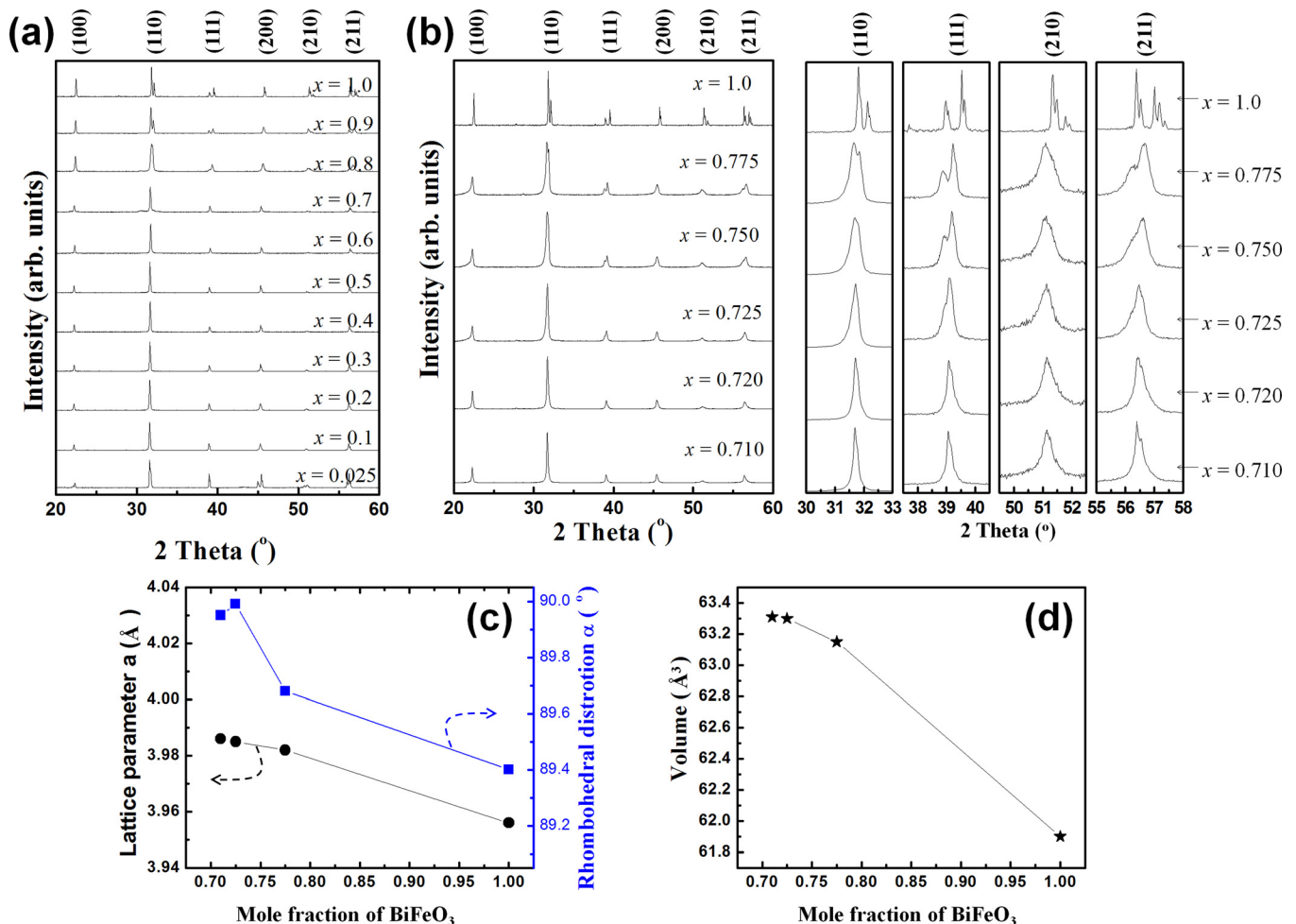


FIG. 1. X-ray diffraction pattern for BT- x BFO ceramics (a) with $x = 0.025 - 1.0$ and (b) with $x = 0.710 - 0.775$ and 1.0, (c) lattice parameter and rhombohedral distortion angle and (d) volume of unit cell for BT- x BFO ceramics with $x = 0.710 - 0.775$ and 1.0.

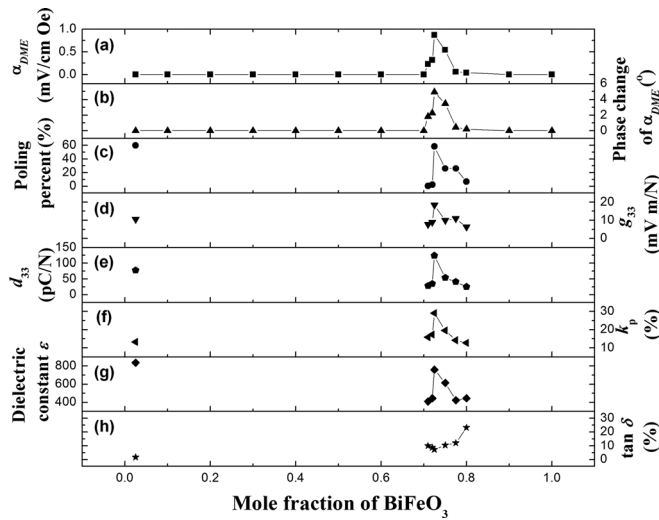


FIG. 2. Variation of magnetoelectric, piezoelectric, and dielectric properties as a function of BFO mole fraction for BT- x BFO ceramics with $x=0.025-1.0$; (a) DME coefficient (α_{DME}), (b) phase change of α_{DME} , (c) poling percent, (d) piezoelectric voltage constant (g_{33}), (e) piezoelectric charge constant (d_{33}), (f) radial mode electromechanical coupling factor (k_p), (g) dielectric constant, (ϵ) and (h) tangent loss factor ($\tan \delta$).

Fig. 2(c), the poling percent ($100 \times (P^0/180^\circ)$), which is determined from the change of phase angle ($P^0 = P_f^0 - P_i^0$), illustrates that the poling was only achieved in the compositions BT- x BFO ($x=0.025$ and $0.710-0.8$) exhibiting tetragonal and rhombohedral phases. Thus, the piezoelectric and dielectric properties can be achieved in the limited range of compositions of BT- x BFO. At the optimum composition of BT- x BFO ($x=0.725$), piezoelectric charge constant (d_{33}), electromechanical coupling factor (k_p), and dielectric constant ($\epsilon = \epsilon^T/\epsilon^0$) were maximized ($d_{33}=124 \text{ pC N}^{-1}$, $k_p=29.1\%$, $\epsilon=760$) and the loss factor ($\tan \delta$) at 1 kHz was minimized ($\tan \delta=7.8\%$) as shown in Figs. 2(e)–2(h). The piezoelectric voltage coefficient ($g_{33} = d_{33}/\epsilon^T$) shown in Fig. 2(d), which is one of the main parameters for achieving high ME coupling was found to be maximized ($g_{33}=18.5 \text{ mV m N}^{-1}$) for the composition BT- x BFO ($x=0.725$). The measured maximum d_{33} (124 pC N^{-1}) of BT-0.725BFO for our samples is quite promising compared with the reported d_{33} (116 pC N^{-1}) for Mn-doped BT-0.75BFO.²⁸ The measured d_{33} (54 pC N^{-1}) of BT-0.75BFO is also comparable with the reported d_{33} (47 pC N^{-1}) of BT-0.75BFO.²⁸ Systematic measurement of d_{33} as a function of composition in our study

led to the identification of BT-0.725BFO composition that provides the best performance. There was no ME response in the BT-0.025BFO due to its small magnetic properties given by low content of Fe ions even though it exhibited good piezoelectric values ($g_{33}=10.5 \times 10 \text{ mV m N}^{-1}$ and $d_{33}=78 \text{ pC N}^{-1}$).

To understand the local structure variation, atomic pair distribution function (PDF) analysis was performed. Fig. 3(a) shows the PDFs for BT-0.725 BFO and BFO ceramic powders. Experimental XRD patterns were taken with Ag radiation ($\lambda=0.56 \text{ \AA}$) and converted into atomic PDFs. The PDFs for pure BFO ($x=1.0$) were fitted with a structure model featuring a rhombohedral structure (S.G. R3c) with lattice parameters in hexagonal setting ($a=5.583 \text{ \AA}$, $c=13.835 \text{ \AA}$, and $\gamma=120^\circ$). The PDFs for BT- x BFO ($x=0.725$) showed better fit at lower r values with a structure model featuring a monoclinic structure (S.G. Cm) with parameters ($a=5.499 \text{ \AA}$, $b=5.631 \text{ \AA}$, $c=3.974 \text{ \AA}$, and $\beta=91^\circ$). At higher r values (see the encircled area), a rhombohedral model (S.G. R3c) ($a=5.558 \text{ \AA}$ and $c=13.834 \text{ \AA}$ and $\gamma=120^\circ$) provided somewhat better fit. Thus, this material can be featured as rhombohedral on average but with local monoclinic distortions/symmetry. Fig. 3(b) shows the polarization-electric field ($P-E$) hysteresis for BT- x BFO ceramics ($x=0.710-0.775$). With increasing BFO mole fraction, the coercive electric field (E_c) was increased up to 36.4 kV cm^{-1} ($x=0.775$) and the remanent polarization (P_r) was also enhanced with high magnitudes of 12.5 ($x=0.725$), 13.8 ($x=0.750$) and $10.9 \mu\text{C cm}^{-2}$ ($x=0.775$). The composition of BT- x BFO ($x=0.725$) was found to exhibit saturated hysteretic curve. Fig. 3(c) shows the magnetization-magnetic field ($M-H$) curves for BT- x BFO ceramics ($x=0.710-0.775$) which were measured under a magnetic field of -7 kOe to $+7 \text{ kOe}$ at room temperature. The $M-H$ curves exhibited linear behavior and no saturation with low magnetic susceptibility (χ) representing insufficient cycloidal spiral in the BT- x BFO solid solutions. With increasing BFO mole fraction from 0.710 to 0.750, the magnetic permeability (μ) was improved and the magnitude of magnetization was increased up to 0.03 emu g^{-1} at 7 kOe for the composition BT- x BFO ($x=0.750$). The improved magnetic properties may be due to the increased amount of Fe ions in the BT- x BFO system. On the other hand, the enhanced magnetic properties with decreasing BFO mole fraction from 0.775 to 0.750 could be attributed to active spin modulation of ordered

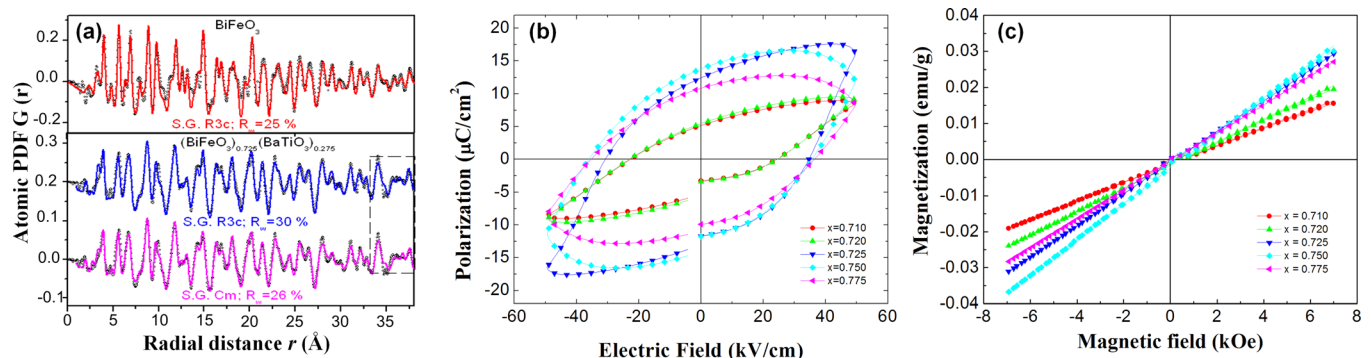


FIG. 3. (a) PDFs analysis, (b) room-temperature $P-E$ curves, and (c) room-temperature $M-H$ curves as a function of BFO mole fraction.

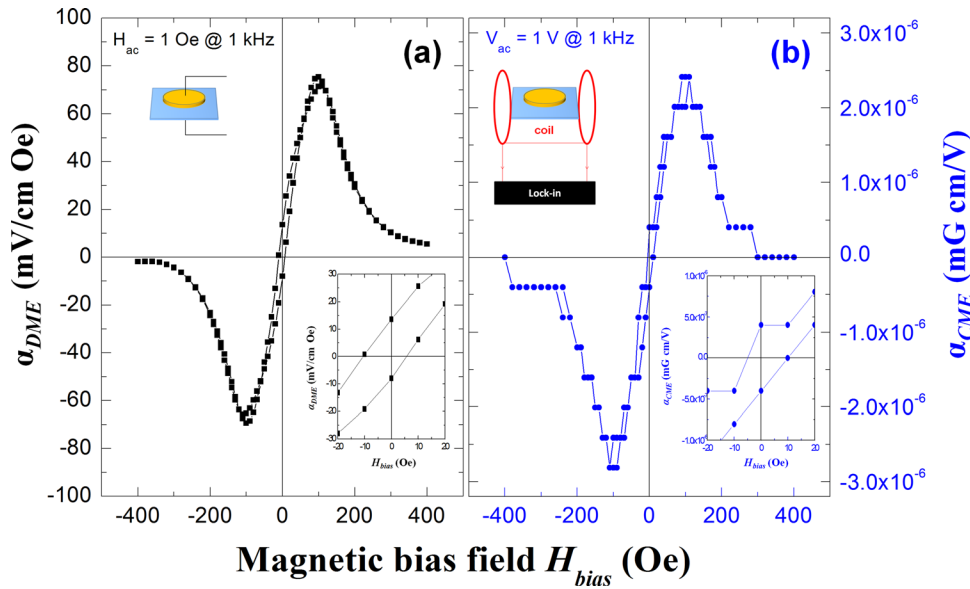


FIG. 4. (a) DME coefficient (α_{DME}) and (b) CME coefficient (α_{CME}) for BT-0.725BFO/Ni laminates as a function of H_{bias} . Insets are schematic diagrams of DME and CME samples and expanded views of $\alpha_{ME}-H_{bias}$ hysteresis to clearly show the remnant α_{DME} and α_{CME} at zero H_{bias} .

Fe-O-Fe. It is illustrated that the substitution of large ions of Ba^{2+} and Ti^{4+} on the A- and B- sites, respectively, may enlarge the distortion of bond angle of Fe-O-Fe to release the spiral magnetic modulation.

Next, BT-0.725BFO/nickel (BT-BFO/Ni) bilayer laminates were fabricated with longitudinally poled and transversely magnetized ($L-T$) configuration to understand the tunability of DME and CME effect. Figs. 4(a) and 4(b) show the DME and CME responses for BT-BFO/Ni laminate. For DME measurement, H_{AC} of 1 Oe at 1 kHz was applied through the Helmholtz coil to the laminate and the induced voltage was measured. Fig. 4(a) shows that the α_{DME} exhibits maximum magnitude of $75.4 \text{ mV cm}^{-1} \text{ Oe}^{-1}$ at H_{bias} of 100 Oe with remnant α_{DME} of $13.6 \text{ mV cm}^{-1} \text{ Oe}^{-1}$ at zero H_{bias} during H_{bias} sweeps. The presence of remnant α_{DME} was realized with exactly the same magnitude by only turning on H_{AC} in the absence of H_{bias} sweep. The result definitely illustrate that the remnant α_{DME} is not a hysteretic characteristic but a spontaneous effect. For CME measurement, V_{AC} of 1 V with 1 kHz was applied directly on the sample and then the induced magnetic flux density was measured by using Helmholtz coil. In the CME response shown in Fig. 4(b), the hysteretic behavior was same with respect to H_{bias} sweep; the maximum α_{CME} was observed with magnitudes of $2.41 \times 10^{-6} \text{ mG cm V}^{-1}$ at $H_{bias} = 100 \text{ Oe}$ and the remnant α_{CME} was obtained with magnitude of $4.02 \times 10^{-7} \text{ mG cm V}^{-1}$ at $H_{bias} = 0 \text{ Oe}$ under applied $V_{AC} = 1 \text{ Oe}$.

IV. CONCLUSION

The lead-free single-phase ME ceramics of BT- x BFO were synthesized by solid solution method. Room-temperature ME coupling was found to exist in the limited composition range of BT- x BFO ($x = 0.71 - 0.8$). The maximum ME coupling coefficient ($\alpha_{ME} = 0.87 \text{ mV/cm-Oe}$) and high piezoelectric properties ($g_{33} = 18.5 \times 10 \text{ mV-m/N}$ and $d_{33} = 124 \text{ pC/N}$) were achieved for the composition BT-0.725 BFO representing local monoclinic distortions in rhombohedral phase. BT-

0.725BFO/Ni laminates were found to exhibit self-biased DME and CME responses, which is very promising for magnetically and electrically tunable on-chip components.

ACKNOWLEDGMENTS

The authors gratefully acknowledge the financial support from ARMDEC (S.-C. Yang) and Office of Naval Research (A. K. and S.P.) through the CEHMS seed program. We appreciate help from Dr. Dwight Viehland (Department of Materials Science and Engineering, Virginia Tech) for VSM measurement.

- ¹R. Ramesh and N. A. Spaldin, *Nature Mater.* **6**, 21–29 (2007).
- ²S. W. Cheong and M. Mostovoy, *Nature Mater.* **6**, 13–20 (2007).
- ³W. Eerenstein, N. D. Mathur, and J. F. Scott, *Nature* **442**, 759–765 (2006).
- ⁴M. Fiebig, *J. Phys. D* **38**, R123–R152 (2005).
- ⁵C.-W. Nan, M. I. Bichurin, S. Dong, D. Viehland, and G. Srinivasan, *J. Appl. Phys.* **103**, 031101–35 (2008).
- ⁶T. Kornev, M. Bichurin, J. P. Rivera, S. Gentil, H. Schmid, A. G. M. Jansen, and P. Wyder, *Phys. Rev. B* **62**, 12247–12253 (2000).
- ⁷G. Lawes and G. Srinivasan, *J. Phys. D: Appl. Phys.* **44**, 243001–243022 (2011).
- ⁸T. R. McGuire, E. J. Scott, and F. H. Grannis, *Phys. Rev.* **102**, 1000–1003 (1956).
- ⁹J. P. Rivera, *Ferroelectrics* **161**, 165–180 (1994).
- ¹⁰J. P. Rivera, *Ferroelectrics* **161**, 147–164 (1994).
- ¹¹G. T. Rado, J. M. Ferrari, and W. G. Maisch, *Phys. Rev. B* **29**, 4041–4048 (1984).
- ¹²B. B. Krichevskov, V. V. Pavlov, and R. V. Pisarev, *JETP Lett.* **49**, 535–539 (1989), available at http://www.jetpletters.ac.ru/ps/1119/article_16956.pdf.
- ¹³C. Ederer and N. A. Spaldin, *Phys. Rev. B* **71**, 060401(1–4) (2005).
- ¹⁴N. Hur, S. Park, P. A. Sharma, J. S. Ahn, S. Guha, and S. W. Cheong, *Nature* **429**, 392–395 (2004).
- ¹⁵J. Ryu, C.-W. Baek, Y.-S. Lee, N.-K. Oh, G. Han, J.-W. Kim, B.-D. Hahn, J.-J. Choi, W.-H. Yoon, J.-H. Choi, D.-S. Park, and D.-Y. Jeong, *J. Am. Ceram. Soc.* **94**, 355–358 (2011).
- ¹⁶J. Ryu, C.-W. Baek, D.-S. Park, and D.-Y. Jeong, *Met. Mater. Int.* **16**, 639–642 (2010).
- ¹⁷K. Ueda, H. Tabata, and T. Kawai, *Appl. Phys. Lett.* **75**, 555–557 (1999).
- ¹⁸M. M. Kumar, S. Srinath, G. S. Kumar, and S. V. Suryanarayana, *J. Magn. Mater.* **188**, 203–212 (1998).
- ¹⁹M. M. Kumar, A. Srinivas, G. S. Kumar, and S. V. Suryanarayana, *J. Phys. Condens. Matter* **11**, 8131–8139 (1999).
- ²⁰W.-M. Zhu, H.-Y. Guo, and Z.-G. Ye, *Phys. Rev. B* **78**, 014401(1–10) (2008).

- ²¹Q. Q. Wang, Z. Wang, X. Q. Liu, and X. M. Chen, *J. Am. Ceram. Soc.* **95**, 670–675 (2012).
- ²²J. Wang, J. B. Neaton, H. Zheng, V. Nagarajan, S. B. Ogale, B. Liu, D. Viehland, V. Vaithyanathan, D. G. Schlom, U. V. Waghmare, N. A. Spaldin, K. M. Rabe, M. Wuttig, and R. Ramesh, *Science* **299**, 1719–1722 (2003).
- ²³Z. M. Tian, Y. S. Zhang, S. L. Yuan, M. S. Wu, C. H. Wang, Z. Z. Ma, S. X. Huo, and H. N. Duan, *Mater. Sci. Eng., B* **177**, 74–78 (2012).
- ²⁴M. M. Kumar, A. Srinivas, and S. V. Suryanarayana, *J. Appl. Phys.* **87**, 855–862 (2000).
- ²⁵J. S. Kim, C. I. Cheon, C. H. Lee, and P. W. Jang, *J. Appl. Phys.* **96**, 468–474 (2004).
- ²⁶T. Sasaki, Y. Hirabayashi, H. Kobayashi, and Y. Sakashita, *Jpn. J. Appl. Phys. (Part 1)* **50**, 09NA08(1–5) (2011).
- ²⁷T. Higuchi, W. Sakamoto, N. Itoh, T. Shimura, T. Hattori, and T. Yogo, *Appl. Phys. Express* **1**, 011502(1–3) (2008).
- ²⁸S. O. Leontsev and R. E. Eitel, *J. Am. Ceram. Soc.* **92**, 2957–2961 (2009).
- ²⁹T.-J. Park, G. C. Papaefthymiou, A. J. Viescas, Y. Lee, H. Zhou, and S. S. Wong, *Phys. Rev. B* **82**, 024431(1–10) (2010).